PROCEEDINGS OF THE ROYAL SOCIETY A

rspa.royalsocietypublishing.org

Research

Cite this article: Ó Náraigh L, Spelt PDM. 2013 An analytical connection between temporal and spatio-temporal growth rates in linear stability analysis. Proc R Soc A 469: 20130171. http://dx.doi.org/10.1098/rspa.2013.0171

Received: 11 March 2013
Accepted: 21 May 2013

Subject Areas:
fluid mechanics

Keywords:
absolute instability, spatio-temporal linear stability, Orr–Sommerfeld equation

Author for correspondence:
Lennon Ó Náraigh
e-mail: lennon.onaraigh@ucd.ie

Electronic supplementary material is available at http://dx.doi.org/10.1098/rspa.2013.0171 or via http://rspa.royalsocietypublishing.org.

Royal Society Publishing
Informing the science of the future

An analytical connection between temporal and spatio-temporal growth rates in linear stability analysis

Lennon Ó Náraigh[1] and Peter D. M. Spelt[2,3]

[1]School of Mathematical Sciences, University College Dublin, Belfield, Dublin 4, Republic of Ireland
[2]Laboratoire de Mécanique des Fluides et d'Acoustique, CNRS, Ecole Centrale Lyon, Ecully, France
[3]Département de Mécanique, Université de Lyon 1, France

We derive an exact formula for the complex frequency in spatio-temporal stability analysis that is valid for arbitrary complex wavenumbers. The usefulness of the formula lies in the fact that it depends only on purely temporal quantities, which are easily calculated. We apply the formula in two model dispersion relations: the linearized complex Ginzburg–Landau equation, and a model of wake instability. In the first case, a quadratic truncation of the exact formula applies; in the second, the same quadratic truncation yields an estimate of the parameter values at which the transition to absolute instability occurs; the error in the estimate decreases upon increasing the order of the truncation. We outline ways in which the formula can be used to characterize stability results obtained from purely numerical calculations, and point to a further application in global stability analyses.

1. Introduction

We consider linear stability analyses of general fluid flows, and begin by recalling the main steps of these, before introducing the motivation of the present work, thereby also introducing the necessary notation. We first restrict ourselves to the linear stability analysis of a parallel flow $U_0(z)$ to two-dimensional disturbances (extensions of the work to non-parallel flows and to three-dimensional disturbances are set out in §6). Such analysis is accomplished by solving the Orr–Sommerfeld (OS) equation [1]. The solution of the equation at

fixed parameter values (such as the Reynolds number Re) yields an eigenvalue problem that connects the wavenumber, the frequency and the growth rate of the disturbance [2]. For two-dimensional disturbances, the perturbation streamfunction has the form $\psi(x,z,t)=\phi(z)\mathrm{e}^{\mathrm{i}(\alpha x-\omega t)}$, where $\alpha=\alpha_\mathrm{r}+\mathrm{i}\alpha_\mathrm{i}$ and $\omega=\omega_\mathrm{r}+\mathrm{i}\omega_\mathrm{i}$ are complex numbers, α_r is the (real) wavenumber, ω_r is the (real) frequency and α_i and ω_i are the spatial and temporal growth rates, respectively; in this context, the OS equation reads

$$\mathrm{i}\alpha(U_0(z)-c)(\partial_z^2-\alpha^2)\phi-\mathrm{i}\alpha U_0''(z)\phi=Re^{-1}(\partial_z^2-\alpha^2)^2\phi,\quad c=\frac{\omega}{\alpha}. \tag{1.1}$$

That the wavenumber α is complex indicates that the instability is spatio-temporal in nature [3]; in a *temporal analysis* [2], $\alpha_\mathrm{i}=0$ and the eigenvalue problem is solved for ω_i and ω_r. This results in the following temporal dispersion relations for the temporal frequency and growth rate, respectively: $\omega_\mathrm{r}^{\mathrm{temp}}=\omega_\mathrm{r}(\alpha_\mathrm{r},\alpha_\mathrm{i}=0)$ and $\omega_\mathrm{i}^{\mathrm{temp}}=\omega_\mathrm{i}(\alpha_\mathrm{r},\alpha_\mathrm{i}=0)$. The basic flow is called *unstable* if the growth rate is positive for some α_r. It is of interest further to classify unstable flows as convectively or absolutely unstable: the flow is convectively unstable if initially localized pulses are amplified in at least one moving frame of reference but are damped in the laboratory frame; on the other hand, the flow is absolutely unstable if such pulses lead to growing disturbances in the entire domain in the laboratory frame.

Briggs [4] developed a method to classify unstable plasmas according to this dichotomy. This criterion has been extended to fluid dynamics by a number of authors [3,5–8]. The approach is based on a *local* eigenvalue analysis of the OS equation, which forms the key ingredient in global analyses: (i) a necessary condition for absolute instability is if the imaginary part of the frequency is positive at a saddle point in the complex α-plane: $\omega_{\mathrm{i}0}:=\omega_\mathrm{i}(\alpha_0)>0$, where α_0 solves $\mathrm{d}\omega/\mathrm{d}\alpha=0$; (ii) to obtain a sufficient condition for absolute instability, the saddle point α_0 in the complex α-plane must be the result of the coalescence of spatial branches that originate from opposite half-planes at a larger and positive value of ω_i (this coalescence or 'pinching' of the spatial branches is accompanied by the formation of a cusp at $\omega_{\mathrm{i}0}$ in the complex ω plane [6]). Typically, the saddle-point and Briggs criteria are checked using a fast numerical eigenvalue solver [9,10]. Our purpose here is not to supplant such effective computations, but rather to develop an analytical connection between spatio-temporal and temporal growth rates to assist in understanding these numerical results. A second motivation is the possible extension of this analytical approach to globally unstable flows. We discuss these motivations in more detail.

Our purpose within a local description is to develop an analytical connection between spatio-temporal and temporal growth rates. Such a connection is desirable for a number of reasons. First, in flows where several temporal modes are unstable, the interpretation of the results of a spatio-temporal stability analysis (obtained numerically, for instance) becomes difficult, as does the mere determination of the convective/absolute (C/A) transitions [11]. In this case, ω-plots of the distinct spatio-temporal modes consist of complicated interpenetrating surfaces, whose domain is the entire complex α-plane. On the other hand, many theoretical tools exist for characterizing temporal instabilities, including energy-budget analyses (as reviewed by Boomkamp & Miesen [12]) and asymptotic analytical solutions [2], so the governing physical mechanisms for growth of temporal modes is often well documented and competing temporal modes can easily be distinguished. A direct link with temporal modes could therefore enable one to distinguish the competing spatio-temporal modes. Furthermore, in parametric studies involving large parameter spaces (e.g. thermal boundary layers or two-phase flows), wherein the C/A transition curves are plotted as a function of the flow parameters, the parametric dependence of the C/A transition curves may be difficult to analyse. For example, for a system with a two-dimensional parameter space (μ_1,μ_2), the curve demarcating the transition between convective and absolute instability is given by the generic formula $\mu_2=f(\mu_1)$. Here, knowledge of the physical properties of the system (in particular, the familiar temporal stability properties) may be beneficial (if not crucial) to deduce the function $f(\cdot)$.

Although the main focus in this study is on an analytic connection between spatio-temporal and temporal local stability growth rates, the results are also of interest in *global* stability analyses. There, the base state can be determined numerically or otherwise (using either an unperturbed solution or a time-averaged perturbed result), in terms of the streamwise coordinate. Assuming this to evolve slowly with the streamwise coordinate the saddle-node frequency, ω_{i0} can then be determined as a function of the real scaled streamwise coordinate, X. But in order to determine global modes (detailed criteria are recalled briefly in §6), $\omega_{i0}(X)$ is required off the real axis, for which analytic continuation is used. In other words, rather than a connection between growth rates for complex and real wavenumbers, one between growth rates for complex and real spatial coordinates is needed. An example of wherein analytical continuation is used for this purpose is the study of Hammond & Redekopp [13]. The formulation proposed herein in the context of a local analysis is readily reformulated for use in this setting for a global analysis, as outlined at the end of this paper, and offers the possibility of developing a combination of both.

This work is organized as follows. We derive an exact formula connecting the spatio-temporal growth rate with purely temporal quantities in §2. We discuss the two lowest-order truncations of this formula in §3: Gaster's formula, and a situation in which the temporal quantities depend only quadratically on the wavenumber α_r. This enables the formulation of condition (i) into a succinct equation encoding the competition between *in situ* growth and convective effects. In §4, we describe the singularities that typically occur in the dispersion relation, and discuss how these can hamper the convergence of our formula. In §5, we apply our results to a simple OS analysis involving wake instability. In §6, we summarize our arguments and describe further applications of the exact formula and its quadratic approximation, including in a global stability analysis.

2. An exact formula for the complex frequency derived from purely temporal quantities

The development of the formula starts with the assumption that an eigenvalue analysis of the OS equation yields a complex frequency ω that depends on the streamwise wavenumber α as an analytic (holomorphic) function, $\omega = \omega_r(\alpha_r, \alpha_i) + i\omega_i(\alpha_r, \alpha_i)$, where we have fixed the other system parameters (e.g. Reynolds number). The domain D of analyticity is an open simply connected subset of $D \subset \mathbb{C}$, containing a part of the real line. Details concerning the domain are discussed further. As a consequence of the analyticity of $\omega(\alpha)$, we have the following Cauchy–Riemann conditions:

$$\frac{\partial \omega_r}{\partial \alpha_r} = \frac{\partial \omega_i}{\partial \alpha_i} \tag{2.1a}$$

and

$$\frac{\partial \omega_r}{\partial \alpha_i} = -\frac{\partial \omega_i}{\partial \alpha_r}. \tag{2.1b}$$

We use equations (2.1*a*,*b*) to derive an expression for $\omega_i(\alpha_r, \alpha_i)$ as a function of the purely temporal stability properties.

We work at a fixed value of α_r in equation (2.1*a*) and identify the group velocity $c_g(\alpha_r) = (\partial\omega_r/\partial\alpha_r)_{(\alpha_r,0)}$. Furthermore, we Taylor-expand $\partial\omega_r/\partial\alpha_r$ into the region D:

$$\frac{\partial \omega_r}{\partial \alpha_r} = \sum_{n=0}^{\infty} \frac{1}{n!} c_{gn}(\alpha_r)\alpha_i^n \quad \text{and} \quad c_{gn}(\alpha_r) = \frac{\partial^n}{\partial \alpha_i^n} \left.\frac{\partial \omega_r}{\partial \alpha_r}\right|_{\alpha_i=0}. \tag{2.2}$$

This amounts to a complex Taylor expansion centred at $(\alpha_r, 0)$ and is therefore valid on a disc of radius R contained entirely in D. The magnitude of the radius of convergence R is discussed below. Each term in this Taylor expansion is available from a purely temporal analysis. We describe this process for the first few terms (for brevity, we use $\partial_i := \partial/\partial\alpha_i$ and $\partial_r := \partial/\partial\alpha_r$).

At $n=0$, we have $c_{g0}=\partial_r\omega_r|_{\alpha_i=0}=c_g(\alpha_r)$, the group velocity. At $n=1$, we obtain

$$c_{g1}=\partial_i\partial_r\omega_r=\partial_r\partial_i\omega_r\overset{\text{C.R.}}{=}-\partial_r\partial_r\omega_i\overset{\alpha_i=0}{=}-\frac{\mathrm{d}^2\omega_i^{\text{temp}}}{\mathrm{d}\alpha_r^2}, \tag{2.3}$$

where ω_i^{temp} is the purely temporal growth rate. At $n=2$, we have

$$c_{g2}=\partial_i\partial_i\partial_r\omega_r=\partial_i\partial_r\partial_i\omega_r\overset{\text{C.R.}}{=}-\partial_i\partial_r\partial_r\omega_i=-\partial_r\partial_r\partial_i\omega_i\overset{\text{C.R.}}{=}-\partial_r\partial_r\partial_r\omega_r\overset{\alpha_i=0}{=}-\frac{\mathrm{d}^2c_g}{\mathrm{d}\alpha_r^2}. \tag{2.4}$$

At $n=3$, we compute

$$\begin{aligned}c_{g3}&=\partial_i\partial_i\partial_i\partial_r\omega_r=\partial_i\partial_i\partial_r\partial_i\omega_r\overset{\text{C.R.}}{=}-\partial_i\partial_i\partial_r\partial_r\omega_i=-\partial_i\partial_r\partial_r\partial_i\omega_i\\&\overset{\text{C.R.}}{=}-\partial_i\partial_r\partial_r\partial_r\omega_r=-\partial_r\partial_r\partial_r\partial_i\omega_r\overset{\text{C.R.}}{=}\partial_r\partial_r\partial_r\partial_r\omega_i\overset{\alpha_i=0}{=}\frac{\mathrm{d}^4\omega_i^{\text{temp}}}{\mathrm{d}\alpha_r^4}.\end{aligned} \tag{2.5}$$

Similarly, at $n=4$, we have

$$\begin{aligned}c_{g4}&=\partial_i\partial_i\partial_i\partial_i\partial_r\omega_r=\partial_i\partial_i\partial_i\partial_r\partial_i\omega_r\overset{\text{C.R.}}{=}-\partial_i\partial_i\partial_i\partial_r\partial_r\omega_i=-\partial_i\partial_i\partial_r\partial_r\partial_i\partial\omega_i\\&\overset{\text{C.R.}}{=}-\partial_i\partial_i\partial_r\partial_r\partial_r\omega_r=-\partial_i\partial_r\partial_r\partial_r\partial_i\omega_r\overset{\text{C.R.}}{=}\partial_i\partial_r\partial_r\partial_r\partial_r\omega_i=\partial_r\partial_r\partial_r\partial_r\partial_i\omega_i\\&\overset{\text{C.R.}}{=}\partial_r\partial_r\partial_r\partial_r\partial_r\omega_r\overset{\alpha_i=0}{=}\frac{\mathrm{d}^4c_g}{\mathrm{d}\alpha_r^4}.\end{aligned} \tag{2.6}$$

We deduce the higher order terms by inspection. Assembling these results, we obtain an expression for $\partial\omega_r/\partial\alpha_r$, extended into the complex plane:

$$\left.\frac{\partial\omega_r}{\partial\alpha_r}\right|_{(\alpha_r,\alpha_i)}=\sum_{n=0}^{\infty}\frac{(-1)^n}{(2n)!}\frac{\mathrm{d}^{2n}c_g}{\mathrm{d}\alpha_r^{2n}}\alpha_i^{2n}+\sum_{n=0}^{\infty}\frac{(-1)^{n+1}}{(2n+1)!}\frac{\mathrm{d}^{2n+2}\omega_i^{\text{temp}}}{\mathrm{d}\alpha_r^{2n+2}}\alpha_i^{2n+1}. \tag{2.7}$$

Next, we use the Cauchy–Riemann condition (2.1*a*) and connect the Taylor expansion in equation (2.7) to an expression for $\omega_i(\alpha_r,\alpha_i)$, valid in the entire complex half-plane $\alpha_r>0$. We have

$$\frac{\partial\omega_i}{\partial\alpha_i}\overset{\text{C.R.}}{=}\frac{\partial\omega_r}{\partial\alpha_r}=\sum_{n=0}^{\infty}\frac{(-1)^n}{(2n)!}\frac{\mathrm{d}^{2n}c_g}{\mathrm{d}\alpha_r^{2n}}\alpha_i^{2n}+\sum_{n=0}^{\infty}\frac{(-1)^{n+1}}{(2n+1)!}\frac{\mathrm{d}^{2n+2}\omega_i^{\text{temp}}}{\mathrm{d}\alpha_r^{2n+2}}\alpha_i^{2n+1}. \tag{2.8}$$

We integrate this relation along a line perpendicular to the real axis, from $(\alpha_r,0)\to(\alpha_r,\alpha_i)$ (α_i is arbitrary, i.e. $|\alpha_i|$ is not necessarily small). The result is

$$\omega_i(\alpha_r,\alpha_i)=\omega_i^{\text{temp}}(\alpha_r)+\sum_{n=0}^{\infty}\frac{(-1)^n}{(2n+1)!}\frac{\mathrm{d}^{2n}c_g}{\mathrm{d}\alpha_r^{2n}}\alpha_i^{2n+1}+\sum_{n=0}^{\infty}\frac{(-1)^{n+1}}{(2n+2)!}\frac{\mathrm{d}^{2n+2}\omega_i^{\text{temp}}}{\mathrm{d}\alpha_r^{2n+2}}\alpha_i^{2n+2}. \tag{2.9}$$

This is an exact formula for the imaginary part of the complex frequency, which depends only on purely temporal quantities. Mathematically, this is a trivial statement: since the complex frequency is analytic, analytic continuation implies that its behaviour on the real line completely determines its behaviour on D. Nevertheless, this formula will help us to create a practical means of predicting the threshold for absolute instability.

The series (2.9) amounts to a complex Taylor series centred at the point $(\alpha_r,0)$ and therefore converges inside a disc of radius R. The radius R is the minimum distance from the point $(\alpha_r,0)$ to the nearest singularity of $\omega(\alpha)$. Care must be taken that the point of interest (e.g. the saddle point of $\omega(\alpha)$) lies inside this disc. A detailed discussion of the radius of convergence of equation (2.9) is given in §4.

3. Low-order truncations and an approximate criterion for the convective/absolute transition

In this section, we investigate the implications of truncating equation (2.9) at linear order and at quadratic order. In the linear truncation, the spatial analysis of Gaster is recovered, while the quadratic truncation applies exactly in model dispersion regulations such as the complex Ginzburg–Landau model. Recovery of these special cases is supplemented with further understanding, namely a 'balance condition' for the onset of absolute instability.

(a) Relation to the analysis of Gaster

The Gaster transformation [14] concerns purely *spatial* instabilities, which correspond to setting $\omega_i = 0$ in the OS eigenvalue analysis, and computing the resulting spatial growth rate α_i as a function of (ω_r, α_r). Practically, this corresponds to a localized disturbance in the flow that oscillates at a characteristic frequency ω_r, and grows downstream of the disturbance at a (spatial) rate $-\alpha_i$. Spatial growth therefore corresponds to negative values of α_i. Using the fact that the general complex frequency $\omega(\alpha)$ is an analytic function, Gaster integrated the resulting Cauchy–Riemann conditions along a straight-line path of small length, $(\alpha_r, 0) \to (\alpha_r, \alpha_i)$, with $|\alpha_i| \ll 1$. The resulting integrands are thus regarded as constant and, setting $\omega_i = 0$, Gaster obtained the following formula for the spatial growth rate:

$$\alpha_i = \frac{-\omega_i^{\text{temp}}}{\mathrm{d}\omega_r^{\text{temp}}/\mathrm{d}\alpha_r}. \tag{3.1}$$

Equation (3.1) provides a precise connection between the spatial growth rate and more familiar temporal quantities. Nevertheless, it is limited, in the sense that it applies only to spatial growth (as opposed to fully spatio-temporal growth) and is valid only for small values of $|\alpha_i|$.

Equation (3.1) can be recovered directly from the approach in §2. Consider equation (2.9) with $|\alpha_i| \ll 1$, such that only the lowest-order term gives a contribution to the equation. The result is

$$\omega_i(\alpha_r, \alpha_i) \sim \omega_i^{\text{temp}}(\alpha_r) + c_g(\alpha_r)\alpha_i, \quad |\alpha_i| \to 0. \tag{3.2}$$

On a spatial branch, we have $\omega_i = 0$, hence equation (3.2) becomes

$$\alpha_i \sim -\frac{\omega_i^{\text{temp}}(\alpha_r)}{c_g(\alpha_r)},$$

as $|\alpha_i| \to 0$, which is precisely the formula of Gaster [14] (equation (3.1)) for spatial modes.

(b) The quadratic approximation

We also derive conditions for the C/A transition based on a second-order truncation of the series dispersion relation (2.9)—the quadratic approximation. In this truncation, the Taylor series (2.9) reduces to

$$\omega_i(\alpha_r, \alpha_i) = \omega_i^{\text{temp}}(\alpha_r) + c_g(\alpha_r)\alpha_i - \frac{1}{2}\frac{\mathrm{d}^2\omega_i^{\text{temp}}}{\mathrm{d}\alpha_r^2}\alpha_i^2. \tag{3.3}$$

The necessary saddle-point condition for an absolute instability (as reviewed in §1) is $\partial\omega_i/\partial\alpha_r = \partial\omega_i/\partial\alpha_i = 0$; using equation (3.3), these conditions amount to

$$\frac{\mathrm{d}\omega_i^{\text{temp}}}{\mathrm{d}\alpha_r} + \frac{\mathrm{d}c_g}{\mathrm{d}\alpha_r}\alpha_i - \frac{1}{2}\frac{\mathrm{d}^3\omega_i^{\text{temp}}}{\mathrm{d}\alpha_r^3}\alpha_i^2 = 0 \quad \text{and} \quad c_g(\alpha_r) - \frac{\mathrm{d}^2\omega_i^{\text{temp}}}{\mathrm{d}\alpha_r^2}\alpha_i = 0. \tag{3.4}$$

Taking the second condition, we get

$$\alpha_i = \frac{c_g(\alpha_r)}{\mathrm{d}^2\omega_i^{\text{temp}}/\mathrm{d}\alpha_r^2}. \tag{3.5}$$

Substitution into the first condition yields

$$c_g(\alpha_r)\frac{dc_g}{d\alpha_r} = -\frac{d\omega_i^{temp}}{d\alpha_r}\frac{d^2\omega_i^{temp}}{d\alpha_r^2} + \frac{1}{2}c_g^2(\alpha_r)\left(\frac{d^3\omega_i^{temp}/d\alpha_r^3}{d^2\omega_i^{temp}/d\alpha_r^2}\right). \tag{3.6}$$

(Note that third-order derivatives appear in this calculation—but only through the process of finding the saddle-point location, and not in the series expansion of the dispersion relation.)

The existence of a real root of equation (3.6) is a necessary condition for a saddle point to occur. Once the root of equation (3.6) is extracted, we derive a condition for the ω_i to vanish at the saddle point, as this is the sign of the transition to absolute instability. Referring to equation (3.3), ω_i vanishes at the saddle when

$$-\left.\frac{d^2\omega_i^{temp}}{d\alpha_r^2}\right|_{\alpha_r^*}\omega_i^{temp}(\alpha_r^*) = \frac{1}{2}c_g^2(\alpha_r^*), \tag{3.7}$$

where α_r^* is the root of equation (3.6). Knowledge of the saddle-point location α_r^*, together with the dispersion relation (3.3) yield further information that can be used to verify if the saddle point arises as a result of the coalescence of spatial branches ramifying into different halves of the complex α-plane (i.e. the necessary and sufficient conditions for the onset of absolute instability). Finally, we note that the dispersion relation for the model linear complex Ginzburg–Landau equation is quadratic in the wavenumber [15,16], and no error is incurred in this case in applying the quadratic truncation of the series dispersion relation (2.9).

(c) Higher order approximations

For certain flows, a higher-order truncation of the series (2.9) may be required, in order to capture the multiplicity of saddle points that can contribute to the spatio-temporal growth in certain anomalous situations [17]. Such singularities may even coalesce into a 'super branch point' [18], determined by the condition $d\omega/d\alpha = d^2\omega/d\alpha^2 = 0$. In this situation, the vanishing of the second derivative of $\omega(\alpha)$ would cause the quadratic approximation to fail, thus further underscoring the importance of developing higher order approximations to the dispersion relation. Such approximations can be obtained by a straightforward extension of the analysis in §3*b*. The reader is referred to the electronic supplementary material for details of an application of the series expansion of the dispersion relation for free-surface flow on an inclined plane [17].

An advantage of the framework developed in this section (compared with the direct approach) concerns the insight given by equation (3.7) into the balance of competing effects that brings about absolute instability. Intuitively, we may think of the condition (3.7) as a competition between *in situ* growth on the left and convection of the disturbance on the right. Absolute instability can set in only if the *in situ* growth equals or exceeds the tendency of the parallel flow to convect disturbances downstream. Similar advantages carry over to situations where high-order truncations are required: the existence of multiple α_i-roots in the polynomial truncation of the criterion $d\omega_i/d\alpha_i = 0$ corresponds exactly to multiple branches in the spatio-temporal growth rate in a moving frame [17]. Finally, we note that although a 'quadratic approximation' was pursued in earlier works, the context was different: either in relation to a numerical, iterative procedure for determining the location of the saddle point (which anyway fails in the presence of multiple saddle points) [19,20], or in the context of asymptotic theories concerned with reduction of a complicated model to a complex Ginzburg–Landau equation [16]. None of these works contains the explicit condition linking the C/A transition to the temporal analysis which is a key result of this section.

4. Convergence of series for ω_i in the presence of a bestiary of singularities

In this section, we review the different kinds of singularity that can occur in the dispersion relation $\omega = \omega(\alpha)$, and discuss the implications of such possible non-analytic behaviour for the

convergence of our formula (2.9). Here, the 'impulse response function' refers to the solution of the spatio-temporal problem

$$\left.\begin{aligned}&[U_0(z)\partial_x+\partial_t](\partial_z^2+\partial_x^2)\psi(x,z,t)-U_0''(z)\partial_x\psi(x,z,t)=Re^{-1}(\partial_z^2+\partial_x^2)^2\psi(x,z,t)\\ \text{and}\quad&\psi(x,z,t=0)=\delta(z)\delta(x).\end{aligned}\right\}\tag{4.1}$$

Equation (4.1) is typically solved using a Laplace–Fourier decomposition; the dispersion relation of the resulting eigenvalue problem (the OS equation) determines the shape of the impulse response.

(a) Branch cuts in unconfined flows

In the so-called *unconfined flows*, the dispersion relation $\omega=\omega(\alpha)$ may possess branch cuts along the imaginary axis $\alpha_r=0$ [8,21]. In such systems (e.g. mixing layers, flow past obstacles), both the streamwise and normal dimensions of the fluid container extend to infinity (labelled by coordinates x and z, respectively), and the disturbance streamfunction decays to zero as $|z|\to\infty$. Then, the asymptotic ($|z|\to\infty$) OS equation reads

$$\mathrm{i}\alpha(U_\infty-c)(\partial_z^2-\alpha^2)\phi=Re^{-1}(\partial_z^2-\alpha^2)\phi,\quad c=\frac{\omega}{\alpha},$$

for a symmetric base state $U_0(z)$ with

$$U_\infty=\lim_{z\to\pm\infty}U_0(z)\quad\text{and}\quad\lim_{z\to\pm\infty}U_0''(z)=0.$$

This asymptotic solution possesses an inviscid mode $\phi\sim\mathrm{e}^{-\mathrm{sign}(\alpha_r)\alpha z}$ and a viscous mode $\phi\sim\mathrm{e}^{-\mathrm{sign}(\gamma_r)\gamma z}$, where $\gamma=\sqrt{\alpha^2+\mathrm{i}\alpha Re(U_\infty-c)}$. The inviscid mode induces a branch cut along the imaginary axis [21], while the viscous mode induces hyperbolic branch cuts in the α-plane [22,23]. All of these branch cuts (or 'continuous spectra' [23]) contribute to the contour integral associated with the impulse-response function. The contour integral of the impulse-response function therefore possesses two contributions: one from the zeros of the dispersion relation $\omega(\alpha)=0$ ('poles'), and the other from the continuous spectrum. However, to diagnose absolute instability, it suffices to consider the discrete part, as the continuous spectrum can produce temporal growth only when the discrete part is absolutely unstable [8].

(b) Discrete poles along the imaginary axis in the complex α-plane

Healey [24,25] has shown that confining an *inviscid* version of the flow described in equation (4.1) between two plates at $z=\pm H$ causes the character of the singularity along the axis $\alpha_r=0$ to switch from a continuous branch cut to a set of discrete poles. For, the inviscid OS (Rayleigh) equation

$$\mathrm{i}\alpha(U_0(z)-c)(\partial_z^2-\alpha^2)\phi-\mathrm{i}\alpha U_0''(z)\phi=0,$$

can be re-written as

$$(\partial_z^2-\alpha^2)\phi=\frac{\mathrm{i}\alpha U_0''(z)\phi}{\mathrm{i}\alpha U_0(z)-\mathrm{i}\omega},$$

such that the singularity $\omega=\infty$ corresponds to $(\partial_z^2-\alpha^2)\phi=0$. This limiting equation satisfies the appropriate boundary conditions for a confined flow (no-penetration at the walls where confinement is enforced) whenever ϕ can be made into an oscillatory function, that is, when $\alpha=\pm n\pi\mathrm{i}/H$, with $n=1,2,\ldots$. These poles induce a series of saddle points near the imaginary axis. These saddle points can dominate over the saddle point associated with the analogous unconfined flow for sufficiently small H. Such saddles can even pinch (according to the Briggs criterion) and thus produce absolute instability [24,25], leading to the conclusion that a confined flow is 'more absolutely unstable' than its unconfined analogue.

Since the introduction of viscosity to the problem does not change the large-ω form of the eigenvalue problem, it is expected that such poles will persist in the viscous case (with some modification of the large-ω streamfunction arising from the different boundary conditions in

the viscous case; J. J. Healey 2012, personal communication). This contention is supported by numerical evidence (§5).

(c) Further branch cuts in the complex α-plane

The generic dispersion relation $\mathcal{D}(\alpha,\omega)=0$ of the OS equation naturally evokes consideration of the multivariable function $\mathcal{D}(\alpha,\omega)$ itself. This is an analytic function in each of its variables [5]. Moreover, $\partial\mathcal{D}/\partial\omega$ has at least one zero [5]. In the neighbourhood of this point (labelled (α_0,ω_0)), $\mathcal{D}(\alpha,\omega)$ can be expanded as

$$\mathcal{D}(\alpha,\omega)=\mathcal{D}(\alpha_0,\omega_0)+\mathcal{D}_\alpha(\alpha_0,\omega_0)(\alpha-\alpha_0)+\tfrac{1}{2}\mathcal{D}_{\omega\omega}(\alpha_0,\omega_0)(\omega-\omega_0)^2+\text{higher order terms},$$

where the subscripts α and ω indicate partial differentiation. If the points (α,ω) and (α_0,ω_0) satisfy the dispersion relation $\mathcal{D}=0$, then this equation can be recast as

$$\omega=\omega_0+\left(-\frac{\mathcal{D}_\alpha(\alpha_0,\omega_0)}{\mathcal{D}_{\omega\omega}(\alpha_0,\omega_0)}\right)^{1/2}(\alpha-\alpha_0)^{1/2}. \tag{4.2}$$

The dispersion relation $\omega(\alpha)$ is therefore non-differentiable at α_0 and possesses a branch cut along a line emanating from the point α_0. Equivalently, one may regard the dispersion relation as being multi-valued, taking distinct values on the two distinct sheets of the Riemann surface described by equation (4.2).

Such singularities can be problematic in a number of ways. First, they limit the radius of convergence of the series dispersion relation (2.9), thus inhibiting the description of a dynamically relevant saddle point via this route. Examples of this kind are found in the works of Brevdo [7] and Juniper [26]. More gravely, if a saddle point of the dispersion relation is sufficiently close to the branch point α_0 in equation (4.2), then in certain situations, the steepest-descent path will intersect the branch cut (no matter how the latter is chosen). In the neighbourhood of this intersection, the function $\omega(\alpha)$ is non-analytic, and the saddle-point method for evaluating the impulse-response integral fails. In this scenario, the saddle point does not produce absolute instability. For an example of this kind, see Lingwood [8]. On the other hand, if the saddle/branch point pair is such that a branch cut can be chosen that does not intersect the steepest-descent contour, then absolute instability occurs [27].

It is clear from this list that knowledge of the global topography of the dispersion relation is required to determine absolute instability (on this point, see also [8]). Equally, such knowledge is necessary to determine when equation (2.9) can be used with confidence. Since equation (2.9) is the imaginary part of a complex-valued power series, it is valid in the disc of convergence of this complex-valued series. The outermost radius R of this disc is given by

$$\begin{aligned}R=&\text{ distance between the point of interest } (\alpha_\mathrm{r},0)\\&\text{and the nearest singularity in } \omega(\alpha);\end{aligned} \tag{4.3}$$

a necessary and sufficient condition for the validity of equation (2.9) at the point $(\alpha_\mathrm{r},\alpha_\mathrm{i})$ is thus $|\alpha_\mathrm{i}|<R$. In practice, the requirement that the global topography of the dispersion relation $\omega(\alpha)$ be known will not limit the potential uses of the local formula (2.9): since we envisage that our formula should be applied to the in-depth analysis of numerical results (for energy-budget analyses and the characterization of mode competition and C/A transition curves [28]), this does not result in any loss of relevance for the formula (2.9).

5. Application of the formula to a canonical fluid instability

The quadratic approximation holds true exactly only for model dispersion relations such as the linearized complex Ginzburg–Landau equation (§3). In more practical systems, the exact series expansion (2.9) would have to converge quickly for the quadratic approximation to be useful. The convergence properties have already been discussed in general terms in §4; here, we discuss

convergence for the particular model (dimensionless) velocity field

$$U_0(z) = 1 - \Lambda + 2\Lambda\{1 + \sinh^{2N}[z\sinh^{-1}(1)]\}^{-1}, \quad \Lambda < 0, \tag{5.1}$$

where Λ and N are dimensionless parameters, and $-\infty < z < \infty$. Equation (5.1) models the steady wake profile generated by flow past a bluff body. The quantity $\Lambda = (U_c - U_{max})/(U_c + U_{max})$ is the velocity ratio, where U_c is the wake centreline velocity and U_{max} is the maximum velocity. Furthermore, N is the shape parameter, which controls the ratio between the mixing-layer thickness and the width of the wake. It ranges from $N = 1$ (the 'sech^2 wake') to $N = \infty$, a 'top-hat wake' bounded by two vortex sheets [20]. The base state (5.1) is absolutely unstable [20] (this serves as a model test case for our purposes; for subsequent work on cylinder wakes, see Pier [29]). The associated OS equation possesses three independent parameters, (Λ, N, Re), where Re is the Reynolds number.

(a) Numerical method

We use a standard Chebyshev collocation method, with ordinary Chebyshev polynomials $\{T_n(\cdot)\}_{n=0}^{N_C}$ as basic functions. Because only the sinuous mode produces absolute instability, the varicose mode is projected out of the problem using appropriate boundary conditions at the symmetry line $z = 0$ [20]. The domain is truncated at $z = H$, with $H = H_c$; the value H_c is large in the sense that the linear-stability results are the same for $H = H_c$ and $H > H_c$. At $z = H$, we force the streamfunction to assume the far-field form $\phi(z) \sim e^{-\alpha z}$. This removes any non-physical saddle points and poles from the numerical solution. These poles would arise if the boundary conditions $\phi = \phi' = 0$ were imposed at $z = H$, and correspond to the 'confinement poles' described in the work of Healey [24,25]. In summary, the following trial solution is assumed for the streamfunction:

$$\phi(z) \approx \sum_{i=0}^{N_C} a_i T_i(\eta), \quad \eta = \frac{2z}{H} - 1, \tag{5.2a}$$

with the following symmetry boundary conditions at $z = 0$:

$$\phi(0) = \phi'''(0) = 0, \tag{5.2b}$$

and the following far-field boundary conditions:

$$\phi'(H) + \alpha\phi(H) = 0 \quad \text{and} \quad \phi''(H) - \alpha^2\phi(H) = 0. \tag{5.2c}$$

The a_i's are determined (along with the eigenvalue $-i\alpha c$) by substitution of equation (5.2*a*) into the OS equation, evaluation at collocation points, and solution of the resulting (finite) matrix eigenvalue problem. Convergence of the numerical method is obtained by increasing N_C until no change in the eigenvalue is observed (to within working precision). The numerical method has been validated by computing the critical Reynolds number for the onset of (convective) instability: $Re_c(N = 1, \Lambda = -1) = 1.8$, and $Re_c(N = 2, \Lambda = -1) = 1.9$, in agreement with the existing literature [20].

(b) Results

Before applying equation (2.9), we perform preliminary studies with the numerical method (5.2). Sample results are shown in figure 1, for the parameter set $(Re, \Lambda, N) = (100, -1.1, 2)$. The method captures the unbounded nature of the problem, in the sense that no confinement poles along the imaginary axis are present. We have verified that replacing the far-field boundary conditions (5.2*c*) by standard no-slip conditions results in a proliferation of poles along the imaginary axis (together with associated saddle points). However, such confinement would be artificial in the context of an unbounded flow, and these no-slip boundary conditions are therefore not considered any further in this context.

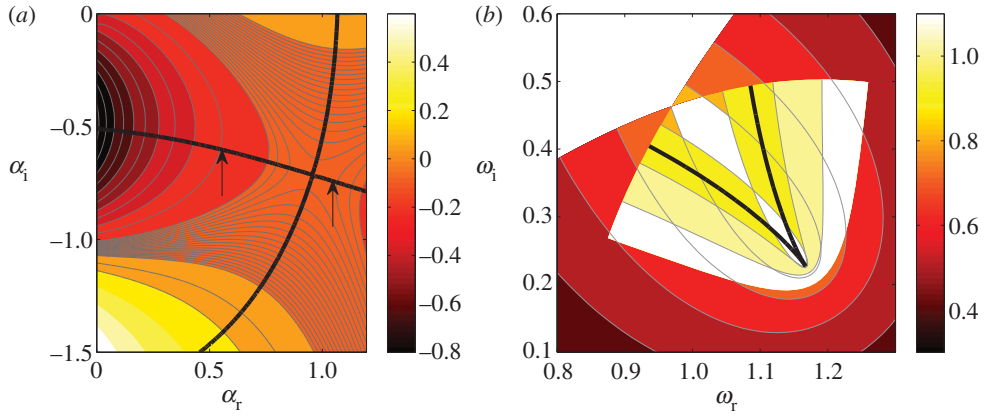

Figure 1. (*a*) The global topography of ω_i for $(Re, \Lambda, N) = (100, -1.1, 2)$. The path of steepest descent through the saddle point is marked by a thick black line with arrows pointing to it. (*b*) The contours of α_r in the complex ω plane. The cusp (thick black line) is a particular contour corresponding to the α_r-value at which the saddle point occurs in (*a*). (Online version in colour.)

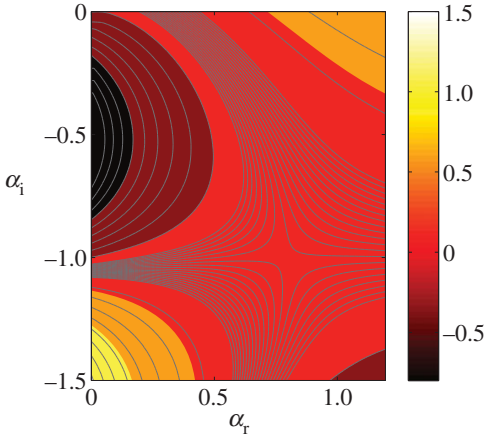

Figure 2. The global topography of ω_i for $(Re, \Lambda, N) = (100, -1.1, 5)$. (Online version in colour.)

In figure 1*a*, a single saddle point exists, with spatial branches ramifying into opposite half-planes. The saddle point therefore satisfies the Briggs criterion for contributing to absolute instability (the ω-cusp [6] at the α-pinchpoint is shown in figure 1*b*). This result was verified further by a so-called *ray analysis* (e.g. the work by Náraigh *et al.* [28]), where the growth rate $\sigma(V)$ along rays moving with velocity V with respect to the laboratory frame is computed from direct numerical simulation of the linearized equations of motion: again, $\sigma(V)$ possesses only one branch, associated with the physical saddle (the reader is referred to the electronic supplementary material for details about such direct numerical simulations). Furthermore, the path of steepest descent is shown in figure 1*a*. The dispersion relation for $(Re, \Lambda, N) = (100, -1.1, 5)$ was found to contain a branch cut emanating from the point $(0.60, -1.95)$. However, this occurred far below the saddle in the complex plane and was not collocated with the steepest-descent path. Consideration of the growth rate $\sigma(V)$ computed via linearized direct numerical simulation showed that this singularity did not contribute to the evolution of an initially localized pulse. A second study with the parameter set $(Re, \Lambda, N) = (100, -1.1, 5)$ was also carried out (figure 2). Although qualitatively very similar to figure 1, the saddle point is located closer to the imaginary axis in this case compared with figure 1; this has implications for the convergence of the series (2.9).

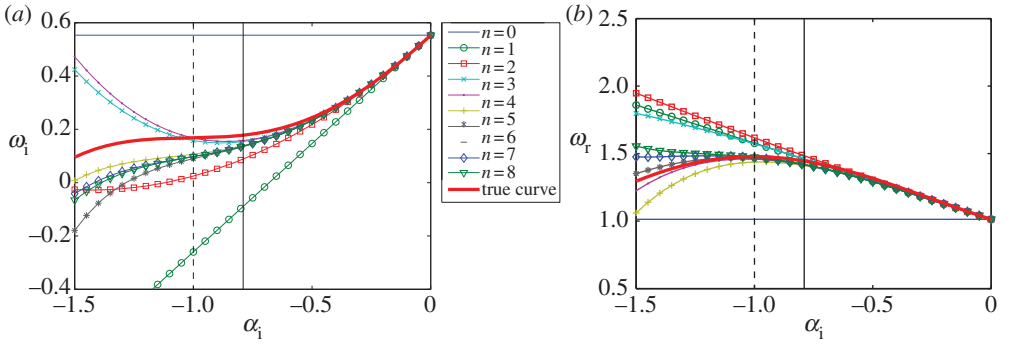

Figure 3. (*a*) Successive truncations of the series for ω_i (equation (2.9)); (*b*) an analogous series for ω_r, and a comparison with the true functions for (ω_r, ω_i). Here, $(Re, \Lambda, N) = (100, -1.1, 5)$, and $\alpha_r = 0.80$, close to the saddle at $(\alpha_r, \alpha_i) = (0.79, -1.0)$. The solid vertical line indicates the radius of convergence, while the broken vertical line indicates the α_i-location of the saddle point. (Online version in colour.)

In figures 1 and 2, the imaginary axis represents a continuous singularity. This can be confirmed by introducing confinement with no-slip conditions at $z = H$: in this case, a series of poles appears on the imaginary axis. In the limit as $H \to \infty$, the poles merge into a continuous singularity, and the unconfined case is recovered. The radius of convergence of the series (2.9) is therefore $R = |\alpha_r|$, where $(\alpha_r, 0)$ is the centre of the series. For a saddle point located at (α_r, α_i), a sufficient condition for the validity of equation (2.9) is thus $|\alpha_i| < |\alpha_r|$. We now consider figures 1 and 2 again. The saddle point is located at $(\alpha_r, \alpha_i) = (0.96, -0.72)$ and $(0.79, -1.0)$ for $N = 2$ and $N = 5$, respectively. It would therefore appear that the series (2.9) converges for the $N = 2$ case and diverges for the $N = 5$ case; however, we have found that high-order truncations of the power series for ω_i (and an analogous series for ω_r) give good approximations to (ω_r, ω_i) outside of this region (figure 3). In certain cases, a truncation of a divergent Taylor series can approximate a function reasonably well. Indeed, for certain cases, there exists an 'optimal truncation', whereby some finite truncation order $N_{\mathrm{trunc,opt}} < \infty$ minimizes the difference between the generating function and the truncated Taylor series.[1] Thus, for physical applications such as the present one, it suffices to determine on a case-by-case basis whether finite truncations of the series for ω_i are good approximations to the underlying function.

Motivated by the good agreement between the true function $\omega_i(\alpha_r, \alpha_i)$ and finite truncations of its Taylor series in figure 3, we have investigated the purely temporal stability properties of the system in figure 3 with a view to applying equation (2.9) to the spatio-temporal problem. This is done in figure 4: the growth rate has the qualitative features of a quadratic equation in α_r. However, the second derivative of the growth rate and the first derivative of the group velocity show strong variation in α_r, and the assumptions of the quadratic approximation do not therefore apply exactly. Consequently, we examine both the quadratic approximation and further, higher order approximations; the latter involve a truncation of equation (2.9) at cubic (or higher) order, together with a procedure analogous to equations (3.3)–(3.7) to obtain the criterion for the onset of absolute instability.

The true boundary between the convective and absolute regions is calculated numerically from a spatio-temporal OS analysis and is identified according to steps (i)–(ii) in §1. The estimated boundary is calculated, according to quadratic and cubic approximations. The quadratic approximation yields a maximum error of 20 per cent with respect to the numerically generated curves. For the cubic approximation, the $Re = 20$ approximate curve and the numerically generated curve virtually coincide, while the maximum error in the $Re = 100$ curve for the cubic

[1]For example, the function $f(x) = (1 + x)\log(1 + x) - x$. On the interval $|x| < 1$, this function can be represented as a power series. However, for $x > 1$, the associated series diverges, but an optimal truncation can be found that minimizes the difference between $f(x)$ and the truncated series.

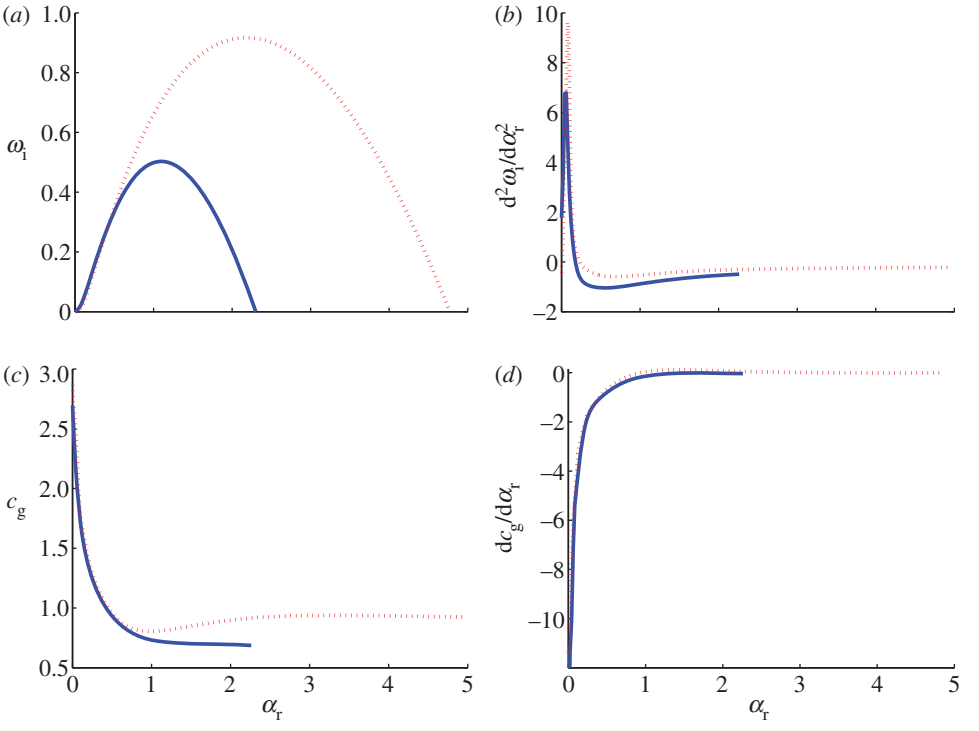

Figure 4. Dispersion curves for two test cases with $(Re, \Lambda) = (100, -1.1)$. Solid line, $N = 2$; dashed line, $N = 5$. The curves for the $N = 2$ case are not continued beyond $\alpha_r \approx 2.3$ because of the significant mode competition (between temporally stable modes) that occurs there. However, this is a region where all modes are stable and is therefore not relevant to the dynamics. (Online version in colour.)

approximation is reduced to 7.5 per cent (figure 5). We have verified that going to higher-order truncations in equation (2.9) for the $Re = 100$ case leads to near-perfect overlap between these curves (a maximum error of 2.5% in a fifth-order truncation, at $Re = 100$).

(c) Interpretation of results via the quadratic approximation

The quadratic approximation can now be used to further analyse the C/A transition. The coefficients in a quadratic approximation for the temporal dispersion relation $\omega_i^{\text{temp}}(\alpha_r)$ can be related to the temporally most-dangerous mode $(\alpha_m, \omega_{im}^{\text{temp}})$, such that

$$\omega_i^{\text{temp}}(\alpha_r) = 2\omega_{im}^{\text{temp}}\left[\frac{\alpha_r}{\alpha_m} - \frac{1}{2}\left(\frac{\alpha_r}{\alpha_m}\right)^2\right], \quad \text{quadratic approximation.} \tag{5.3}$$

Moreover, we have found in our numerical calculations that the α_r-location of the unstable saddle point in the complex dispersion relation almost coincides with the most-dangerous mode, such that (using the notation in §3*b*) $\alpha_r^* \approx \alpha_m$. The criterion (3.7) in §3*b* describing the onset of absolute instability then reduces to

$$\frac{2\omega_{im}^{\text{temp}}}{\alpha_m} = c_g(\alpha_m). \tag{5.4}$$

Both sides of the condition (5.4) are well represented by expressions of the form $A(N, Re) + B(N, Re)\Lambda$ over the part of parameter space considered in §5*b*. In figure 6, the dependencies of these coefficients on N and Re are shown. The most significant of these is the N-dependency of the coefficient B for the group velocity: increasing N makes the group velocity approach unity

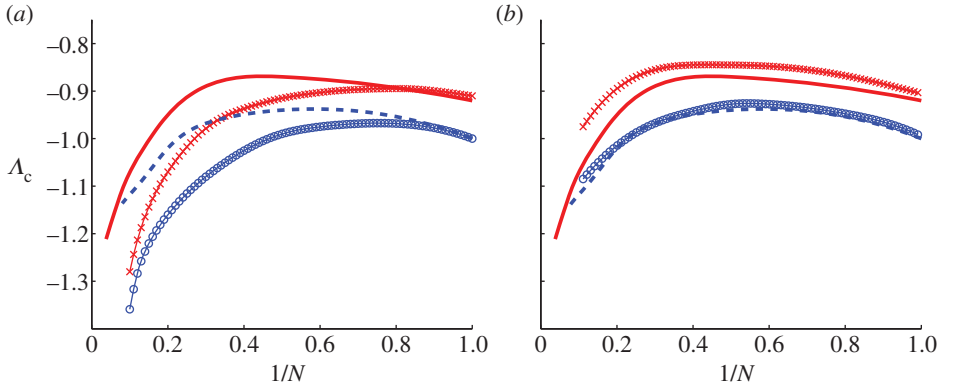

Figure 5. Boundary between the absolute and convective regions for different Reynolds numbers, with comparison to the (*a*) quadratic and (*b*) cubic approximations. Curves without symbols correspond to direct OS eigenvalue calculations in the complex α-plane and agree exactly with the results by Monkewitz [20]. Dashed curve, $Re = 20$; solid curve, $Re = 100$. Circles, approximate curves at $Re = 20$; crosses, approximate curves $Re = 100$. (Online version in colour.)

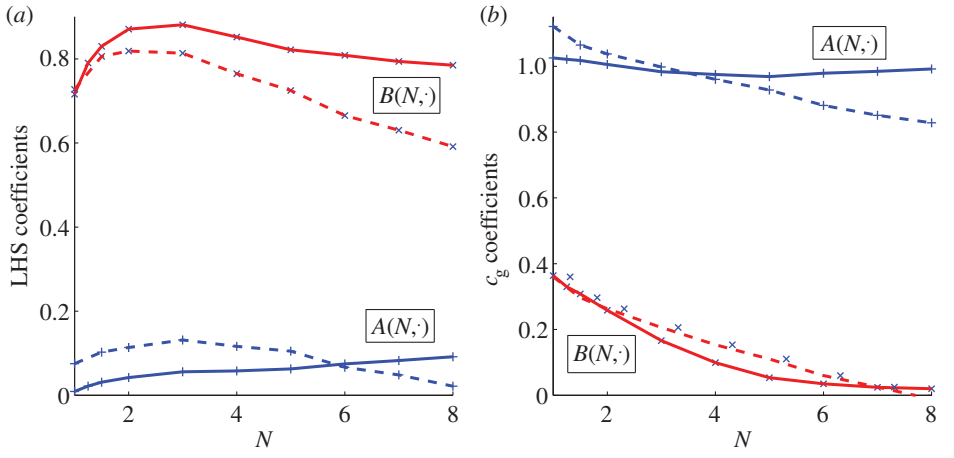

Figure 6. Dependency on N of coefficients in fits linear in Λ of the left-hand side of equation (3.7) (*a*) and the group velocity (*b*) at $Re = 100$ (solid lines) and $Re = 20$ (dashed lines); plus symbols and crosses represent A and B, respectively. In (*a*), the sign of both coefficients has been reversed. (Online version in colour.)

rapidly from below. If we ignore for the time being the other dependencies on N and use for the left-hand side of equation (5.4) simple N-averaged values ($A \equiv a_0 \approx -0.05$ and $B \equiv a_1 \approx -0.8$ for $Re = 100$), and for the group velocity the curve fit

$$c_g(\alpha_m) \approx 1 + b_0 \exp(-b_1 N)\Lambda \tag{5.5}$$

(with $b_0 \approx 0.6$ and $b_1 \approx 0.5$ for $Re = 100$), we obtain an approximate expression for the C/A transition based on the quadratic approximation:

$$\Lambda_{CA} \approx \frac{a_0 - 1}{b_0 \exp(-b_1 N) - a_1}. \tag{5.6}$$

We have found this to represent the full results obtained with the quadratic approximation within the uncertainty of the value of the coefficients. Overall then, the main trend is that in making Λ more negative, the group velocity (the right-hand side of equation (5.4)) decreases, whereas the

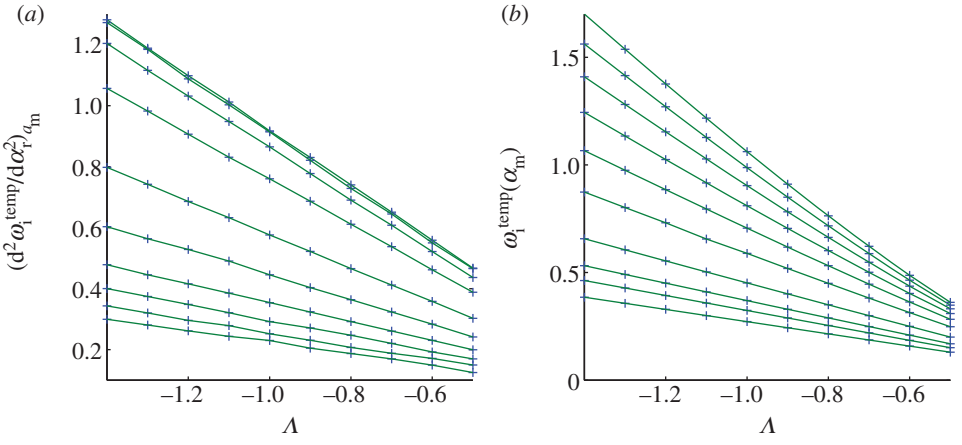

Figure 7. The dependencies on N and Λ of (*a*) $-\mathrm{d}^2\omega_\mathrm{i}^\mathrm{temp}/\mathrm{d}\alpha_\mathrm{r}^2$; (*b*) $\omega_\mathrm{i}^\mathrm{temp}$, at the most-dangerous temporal mode for $Re = 100$. Results are shown for $N = 1, 1.25, 1.5, 2, 3, 4, 5, 6, 7, 8$ from top to bottom in (*a*), and from bottom to top in (*b*). (Online version in colour.)

left-hand side of equation (5.4) increases; these two effects promote absolute instead of convective instability. Thus, the steep drop in the curves at large N in figure 5 is associated with the fact that increasing N increases the group velocity.

Regarding the dependencies on Re, we first note that at low values of N, the magnitude of the left-hand side of equation (5.4) is small at $Re = 20$ compared with $Re = 100$, whereas the magnitude of the right-hand side is large; these changes both favour convective instability. At intermediate-to-large values of N, both terms decrease when the value of Re is decreased, with the left-hand side more so than the right-hand side. Hence, the C/A transition in figure 5 occurs at a more negative value of Λ for the lowest value of Re due to effects on both sides in equation (5.4). These effects can be accounted for in the above through the introduction of explicit Re-dependencies in the coefficients a_0, a_1, b_0, b_1 (even if only representing the Re-dependencies of their N-averaged values). These dependencies are already visible in figure 6, although their parametrization is beyond the scope of this paper.

These somewhat crude approximations can be refined by representing the dependency of the left-hand-side coefficients A and B on N, the causes of which we first briefly investigate here. At values of N near unity, the magnitude of the left-hand side of equation (5.4) first increases strongly with N before decreasing beyond $N \approx 3$, such that the region of absolute instability in parameter space is reduced further at large values of N. In fact, the results in figure 6*a* convey two different stories, for values below and above $N = 3$. Referring back to equation (3.7), we recall that the left-hand side is the product of the maximum temporal growth rate and minus the curvature of the dispersion relation. Results for these two components are shown in figure 7. We conclude from figure 7 that $\omega_\mathrm{i}^\mathrm{temp}(\alpha_\mathrm{m})$ increases uniformly with increasing N, consistent with the increase in the entire left-hand side of equation (3.7) at low values of N, and that the resulting promotion of absolute instability is only reversed by a decrease in $-\mathrm{d}^2\omega_\mathrm{i}^\mathrm{temp}/\mathrm{d}\alpha_\mathrm{r}^2$ at large values of N; at low values of N, this curvature term hardly depends on N. It is possible to account for these trends in equation (5.6), by using bilinear fits for $\omega_{\mathrm{i}\,\mathrm{m}}^\mathrm{temp}$ and α_m (as well as equation (5.5) for the group velocity):

$$\alpha_\mathrm{m} \approx a_\alpha^0 + a_\alpha^1 N + b_\alpha^0 \Lambda + b_\alpha^1 N\Lambda \quad \text{and} \quad \omega_{\mathrm{i}\,\mathrm{m}}^\mathrm{temp} \approx a_\omega^0 + a_\omega^1 N + b_\omega^0 \Lambda + b_\omega^1 N\Lambda. \tag{5.7}$$

Substitution of equation (5.7) into equation (5.4) then yields a quadratic equation for Λ at the C/A transition. This whole approach can be extended by lifting the approximation $\alpha_\mathrm{r}^* \approx \alpha_\mathrm{m}$, or by going to higher-order truncations of the dispersion relation; however, these complications obscure

the understanding achieved here using simple linear and bilinear fitting, and such extensions are not pursued further here.

6. Discussion

We have presented an analytical connection between spatio-temporal and temporal growth rates in a local linear stability analysis. Specifically, we have derived criteria for a transition between convective and absolute instability, explicitly in terms of the temporal problem, to increasingly refined levels of approximation. The simplest approximation is a quadratic one where the location of the saddle α_r^* is assumed to coincide with the temporally most-dangerous mode; then, the criterion for the onset of absolute instability is given by equation (5.4). At the next level of approximation (still quadratic), one determines α_r^* via equation (3.6). Although this approach can be used directly to determine C/A transitions, we anticipate that the main use of the theory will be in analysing results obtained with an efficient computational algorithm for the full OS problem. We imagine that one would perform such a numerical calculation, diagnose absolute instability (using the saddle-point/pinch-point criteria), and then characterize the instability in detail. Our formula can help in this characterization in the following ways. First, in parametric studies, the dependency of C/A transition curves on model parameters can be difficult to analyse, especially if there are many governing parameters. In §5, we have seen an example wherein simple approximations based on equation (2.9), together with insight into the trends exhibited by the dispersion relation in the purely temporal problem, yield a detailed explanation of the behaviour of the C/A transition curves. Additionally, given the analytic connection between temporal and spatial growth in equation (2.9), it follows that features in contour plots for a spatio-temporal growth rate (such as saddle points) can be related directly to a specific temporal mode with the present approach. The advantage of this is that such features can then be associated with the physical mechanism which governs that temporal mode. The application of the approach proposed here to real flows has recently been completed by Ó Náraigh *et al.* [28], where we have studied absolute and convective instability in two-phase gas/liquid flows. There, however, the focus was on the application of the theory in a detailed parameter study and a derivation of the quadratic approximation was not included; in the present work, the focus is on the mathematical derivation of equation (2.9), discussion of the radius of convergence of the formula, and the investigation of the accuracy of finite truncations of the equation (2.9). Such analysis is important before the theory can be used with confidence in further applications.

Throughout this paper, we have considered two-dimensional disturbances, taking ω as a complex-valued function of a single complex variable (the complex wavenumber). However, this approach could be extended to three-dimensional spatio-temporal disturbances, via a double-Taylor-series expansion of the dispersion relation in the streamwise and spanwise wavenumbers. For cases wherein the spanwise wavenumber is real, the analysis presented herein requires no modification, as the spanwise wavenumber would then only enter as an additional parameter.

We conclude by discussing briefly a further application of this method to weakly globally unstable modes. In non-parallel flows, the properties of the system vary in the streamwise direction, and a standard normal-mode decomposition is no longer possible. The generic linear-stability problem to be solved then reads $\partial_t \psi = \mathcal{L}(\partial_x, \partial_z)\psi$, where $\mathcal{L}$ is a linear operator with coefficients that depend on the streamwise direction; the normal-mode decomposition $\partial/\partial x \rightarrow \mathrm{i}\alpha$ is no longer possible. We make trial substitution $\psi \rightarrow \psi(x,z)\mathrm{e}^{-\mathrm{i}\omega_G t}$ and obtain the global eigenvalue problem, $\mathrm{i}\omega_G \psi(x,z) = \mathcal{L}(\partial_x, \partial_z)\psi(x,z)$. The system is globally unstable if there exists a global mode for which $\Im(\omega_G) > 0$. We introduce a parameter $\varepsilon = \lambda/L$, where λ is the typical length scale of the disturbance ψ, and L is a measure of the system's extent in the streamwise direction. If $\varepsilon \ll 1$, and if the coefficients of the linear operator $\mathcal{L}$ depend only weakly on space, through the combination $X := \varepsilon x$, then a WKB (Wentzel–Kramers–Brillouin) approximation [3,23,30] can be used to demonstrate that the leading-order approximation to the most-dangerous global mode is $\omega_G = \omega_0(X_s) + O(\varepsilon)$, where $\omega_0(X_s)$ is the saddle-point frequency calculated in the usual manner from a purely *local* stability analysis, at the fixed parameter value X_s, and X_s is the location of the

saddle point of the complex-valued function $\omega_0(X)$ in the complex X-plane: $(\partial\omega_0/\partial X)(X_s) = 0$. The flow is therefore globally unstable if $\omega_0(X_s) > 0$. Thus, we are interested in a prescribed complex-valued function of a complex variable, $\omega_0(X)$, and its saddle point(s). If $\omega_0(X)$ is holomorphic, and if $\omega_0(X)$ is known along the real line, then the arguments of §2 also apply to the function $\omega_0(X)$, and the following formula pertains:

$$\omega_{0\mathrm{i}}(X_\mathrm{r}, X_\mathrm{i}) = \omega_{0\mathrm{i}}(X_\mathrm{r}, X_\mathrm{i} = 0) + \sum_{n=0}^{\infty} \frac{(-1)^n}{(2n+1)!} \frac{\mathrm{d}^{2n+1}}{\mathrm{d}X_\mathrm{r}^{2n+1}} [\omega_{0\mathrm{r}}(X_\mathrm{r}, X_\mathrm{i} = 0)] X_\mathrm{i}^{2n+1} + \sum_{n=0}^{\infty} \frac{(-1)^{n+1}}{(2n+2)!} \frac{\mathrm{d}^{2n+2}}{\mathrm{d}X_\mathrm{r}^{2n+2}} [\omega_{0\mathrm{i}}(X_\mathrm{r}, X_\mathrm{i} = 0)] X_\mathrm{i}^{2n+2}. \tag{6.1}$$

Furthermore, if $\omega_0(X)$ is quadratic in X, then the truncation in §3*b* applies, and the condition for the onset of global instability reads

$$-\left[\frac{\mathrm{d}^2\omega_{0\mathrm{i}}(X_\mathrm{r}, X_\mathrm{i} = 0)}{\mathrm{d}X_\mathrm{r}^2}\right]_{X_\mathrm{r}^*} \omega_{0\mathrm{i}}(X_\mathrm{r}^*, X_\mathrm{i} = 0) = \frac{1}{2}\left[\frac{\mathrm{d}\omega_{0\mathrm{r}}(X_\mathrm{r}, X_\mathrm{i} = 0)}{\mathrm{d}X_\mathrm{r}}\right]_{X_\mathrm{r}^*}^2, \tag{6.2}$$

where X_r^* satisfies a root-finding condition analogous to equation (3.6). A first-order truncation equation (6.1) was used in [13], with $\omega_{0\mathrm{i}}(X_\mathrm{r}, X_\mathrm{i} = 0)$ determined numerically. The present approach would not only allow for rapid extension to higher order, but also open up the possibility of using equation (6.2) in conjunction with, for instance, the local quadratic approximation (3.7) to determine the terms that make up equation (6.2).

This research was supported by the Ulysses-Ireland/France Research Visits Scheme, a programme for research visits between Ireland and France, jointly funded and administered by The Irish Research Council, the Irish Research Council for Science Engineering and Technology and Egide, the French agency for international mobility, with participation from the French Embassy in Ireland and Teagasc.

L.Ó.N. would like to thank many people for extremely helpful and cordial discussions: R. Smith, C. Boyd, J. J. Healey, and two anonymous referees. P.S. would like to acknowledge useful discussions with his colleague B. Pier.

References

1. Orr WM'F. 1907 The stability or instability of the steady motions of a liquid. Parts I–II. *Proc. R. Irish Acad. A* **27**, 9.
2. Drazin PG, Reid WH. 1981 *Hydrodynamic stability*. Cambridge, UK: Cambridge University Press.
3. Huerre P, Monkewitz PA. 1990 Local and global instability in spatially developing flows. *Ann. Rev. Fluid Mech.* **22**, 473–537. (doi:10.1146/annurev.fl.22.010190.002353)
4. Briggs RJ. 1964 *Electron-stream interactions with plasmas*. Cambridge, MA: MIT Press.
5. Gaster M. 1968 Growth of disturbances in both space and time. *Phys. Fluids* **11**, 723. (doi:10.1063/1.1691990)
6. Kupfer K, Bers A, Ram AK. 1987 The cusp map in the complex-frequency plane for absolute instabilities. *Phys. Fluids* **30**, 3075. (doi:10.1063/1.866483)
7. Brevdo L. 1988 A study of absolute and convective instabilities with an application to the Eady model. *Geophys. Astrophys. Fluid Dyn.* **40**, 1–92. (doi:10.1080/03091928808208820)
8. Lingwood RJ. 1997 On the application of the Briggs' and steepest-descent methods to a boundary-layer flow. *Stud. Appl. Math.* **98**, 213–254. (doi:10.1111/1467-9590.00048)
9. Boyd JP. 2001 *Chebyshev and Fourier spectral methods*. New York, NY: Dover.
10. Trefethen LN. 2000 *Spectral methods in MATLAB*. Philadelphia, PA: SIAM.
11. Suslov SA. 2006 Numerical aspects of searching convective/absolute instability transition. *J. Comput. Phys.* **212**, 188–217. (doi:10.1016/j.jcp.2005.06.017)
12. Boomkamp PAM, Miesen RHM. 1996 Classification of instabilities in parallel two-phase flow. *Int. J. Multiphase Flow* **22**, 67–88. (doi:10.1016/S0301-9322(96)90005-1)
13. Hammond DA, Redekopp LG. 1997 Global dynamics of symmetric and asymmetric wakes. *J. Fluid Mech.* **331**, 231–260. (doi:10.1017/S0022112096003825)

14. Gaster M. 1962 A note on the relation between temporally-increasing and spatially-increasing disturbances in hydrodynamic instability. *J. Fluid Mech.* **14**, 222–224. (doi:10.1017/S0022112062001184)
15. Huerre P. 2000 Open shear flow instabilities. In *Perspectives in fluid mechanics* (eds GK Batchelor, HK Moffatt, MG Worster), pp. 182–186. Cambridge, UK: Cambridge University Press.
16. Suslov SA, Paolucci S. 2004 Stability of non-Boussinesq convection via the complex Ginzburg–Landau model. *Fluid Dyn. Res.* **35**, 159. (doi:10.1016/j.fluiddyn.2004.06.002)
17. Brevdo L, Laure P, Dias F, Bridges TJ. 1999 Linear pulse structure and signalling in a film flow on an inclined plane. *J. Fluid Mech.* **396**, 37–71. (doi:10.1017/S0022112099005790)
18. Healey JJ. 2004 On the relation between the viscous and inviscid absolute instabilities of the rotating-disk boundary layer. *J. Fluid Mech.* **511**, 170. (doi:10.1017/S0022112004009565)
19. Deissler RJ. 1987 The convective nature of instability in plane Poiseuille flow. *Phys. Fluids* **30**, 2303–2305. (doi:10.1063/1.866118)
20. Monkewitz PA. 1988 The absolute and convective nature of instability in two-dimensional wakes at low Reynolds numbers. *Phys. Fluids* **31**, 999. (doi:10.1063/1.866720)
21. Huerre P, Monkewitz PA. 1985 Absolute and convective instability in free shear layers. *J. Fluid Mech.* **159**, 151–168. (doi:10.1017/S0022112085003147)
22. Aships DE, Reshotko E. 1990 The vibrating ribbon problem revisited. *J. Fluid Mech.* **213**, 531–547. (doi:10.1017/S0022112090002439)
23. Schmid PJ, Henningson DS. 2001 *Stability and transition in shear flows*. New York, NY: Springer.
24. Healey JJ. 2007 Enhancing the absolute instability of a boundary layer by adding a far-away plate. *J. Fluid Mech.* **579**, 29–61. (doi:10.1017/S002211200700482X)
25. Healey JJ. 2009 Destabilizing effects of confinement on homogeneous mixing layers. *J. Fluid Mech.* **623**, 241–271. (doi:10.1017/S0022112008005284)
26. Juniper MP. 2006 The effect of confinement on the stability of two-dimensional shear flows. *J. Fluid Mech.* **565**, 171–195. (doi:10.1017/S0022112006001558)
27. Healey JJ. 2006 A new convective instability of the rotating-disk boundary layer with growth normal to the disk. *J. Fluid Mech.* **560**, 279–310. (doi:10.1017/S0022112006000504)
28. Ó Náraigh L, Spelt PDM, Shaw SJ. 2013 Absolute linear instability in laminar and turbulent gas/liquid two-layer channel flow. *J. Fluid Mech.* **714**, 58–94. (doi:10.1017/jfm.2012.452)
29. Pier B. 2002 On the frequency selection of finite-amplitude vortex shedding in the cylinder wake. *J. Fluid Mech.* **458**, 407–417. (doi:10.1017/S0022112002008054)
30. Chomaz J-M, Huerre P, Redekopp LG. 1991 A frequency selection criterion in spatially developing flows. *Stud. Appl. Math.* **84**, 119.